Effects of laser irradiation on the microstructure and surface morphology of zinc oxide doped with different additives

M. Y. Helali[1,*], M. M. Saadeldin[2] and Makram Ibrahim[3]

[1]Space Research Laboratory, National Research Institute of Astronomy and Geophysics, EL Marsad Street 1, Helwan, Cairo, Egypt
[2]Physics Department, Faculty of Science, Cairo University, 1 Gamaa Street, Giza, Egypt 12613
[3]Solar and Space Research Department, National Research Institute of Astronomy and Geophysics, EL Marsad Street 1, Helwan, Cairo, Egypt

Zinc oxide (ZnO) disc samples doped with copper oxide as the main impurity were prepared and irradiated for 2 min by 1.064 μm semi-train of 20 ps pulses having energy of 80 mJ in a spot size of 5 mm diameter and average pulse power density of about 1.3 GW/cm^2. X-ray diffraction reveals a large increase in the average crystallite size after laser irradiation for 2 min, which leads to a consequent large decrease in the average dislocation as it is inversely proportional to the square of the crystallite size. Scanning electron microscopy images show the presence of inter-granular phase and CuO particles between the ZnO grain boundaries. They also show a noticeable decrease of ZnO grain size after laser irradiation for 2 min due to grain melting. Atomic force microscopy shows increase in the roughness after laser irradiation. The laser irradiation of samples also resulted in the destruction of ZnO surface hexagonal structure with large increase of inter-granular spaces, which may be due to grain melting. The laser-induced grain melting also resulted in increasing roughness and in forming pores, cracks and particulates with dimensions comparable to average grain size. The binding energies of Zn 2p, Cu 2p, Cr 2p and O 1s core levels of ZnO varistor surfaces were determined for one sample by X-ray photoelectron spectroscopy.

Keywords: Laser irradiation, microstructure, surface morphology, X-ray diffraction, zinc oxide.

IN recent years, laser irradiation has emerged as a powerful method for modifying the properties of material surfaces. However, conventional furnace annealing and rapid thermal annealing are widely known as effective techniques to improve the crystalline quality. Compared with the classic annealing method, the laser irradiation technique provides some distinctive advantages, such as rapid local heating, reduced thermal exposure of the sample and flexible management[1–3]. Since the invention of lasers in 1960 till 1990, the preferred lasers in materials science were the CO_2 laser at a wavelength of 10.6 μm and the Nd : YAG laser at 1.064 μm, both of which are in the infrared (IR) spectral region. Thereafter, the field of laser–solid interaction has undergone tremendous development with more intense and reliable ultra-short pulsed lasers[4]. The interaction of a laser beam and a solid material is generally characterized by one or more of the four well-known processes which can occur simultaneously: reflection, absorption, scattering and transmission. However, only the absorbed photons in a laser–matter interaction can affect the physical and chemical properties of any material. Zinc oxide (ZnO) is a wide band-gap semiconductor ceramic material; at room temperature it has a direct band gap of 3.37 eV. ZnO has important applications such as varistors, UV light-emitting diodes and transparent field-effect transistors. It also possesses many unique properties for other applications, such as solar cells, surface acoustic wave devices, gas sensors[5–8], and is an essential ingredient of rubber mixes, some ceramic goods and paints[9]. In previous studies[10,11], important applications of ZnO–CuO were analysed for gas detection and nanophotocatalysts. All of these applications are either dependent upon or are affected by impurities and defects. The effect of temperature on the characteristics of ZnO with cerium oxide at constant frequency (20 kHz) was studied in 2013; new ZnO varistors doped with rare earth elements have also been studied[12,13]. As varistors, they are widely used in electrical circuits against dangerous voltage surges. ZnO crystallizes in the hexagonal wurtzite lattice in which oxygen ions are arranged in the closest hexagonal packing, and zinc ions occupy half of the tetrahedral interstitial positions and have the same relative arrangement as the oxygen ions. Metal–oxide varistors were initially developed in Japan and are available in USA since 1972 (ref. 14). ZnO varistors are highly complex, polycrystalline oxide ceramics with highly nonlinear current–voltage characteristics[15] whose electrical behaviour depends both on the microstructure of the device and on the detailed processes occurring at the ZnO grain boundaries. The primary constituent of such a varistor is obviously ZnO, typically 90% or more. In addition, the varistor contains smaller amounts of other constituents such as metal oxides. The

*For correspondence. (e-mail: mohelay71@gmail.com)

varistor nonlinear property is related to conduction mechanism in the inter-granular phase, where conduction depends on the electronic structure in the vicinity of the grain boundaries. In the present study three disc samples of bulk ZnO doped with CuO were prepared and their microstructures studied by X-ray diffraction (XRD), scanning electronic microscope (SEM) and atomic force microscope (AFM) characterization tools before and after laser irradiation. The main aim of this study is to examine the laser irradiation effect on the microstructure and surface morphology of ZnO varistor material doped with CuO. This allows study of the effect of laser-induced microstructure and surface modification on the electrical properties such as conductivity, nonlinearity and *V–I* characteristics.

Experimental work

The experimental work consists mainly of three regimes, namely sample preparation, laser system and irradiation of the samples, and material characterization both before and after laser irradiation.

Sample preparation

The sintered polycrystalline samples were prepared by conventional ceramic fabrication procedures. Reagent-grade ZnO, CuO powders were mixed by wet ball-milling using deionized water. The three bulk disc specimens (1–3) were compressed under a force of 70 kN, dried and then fired at 1100°C for 2 h. Specimens were first polished with different grades of diamond paste, thoroughly washed in an ultrasonic bath, dried and then thermally etched at 1000°C for 30 min (ref. 16). The CuO additives (mol%) are 0.5 for sample 1, 1.0 for sample 2 and 3.0 for sample 3. Figure 1 is a block diagram showing the steps for preparation of ZnO varistors.

Laser system and set-up for irradiation

The laser system used to irradiate the samples under study is a Nd : YAG picosecond mode-locked flash-lamp pumped laser system. It was designed and constructed by the Czech Technical University in Prague, Czech Republic, for use in SLR (satellite laser ranging) in Helwan city, Egypt[17,18]. Figure 2 shows a block diagram of the Nd : YAG laser system and set-up for irradiating the samples with the mode-locked semi-trains of 20 ps pulses. In the figure, M_0 is a silvered total reflecting mirror for the He–Ne laser used to align the Nd : YAG system, M_1–M_8 are total dielectric reflecting mirrors for 1.064 μm radiation[19]. The oscillator consists of an optical resonator, active medium side-pumped by a flash-lamp, and a dye cell. The dye cell contains 2 cm^3 of dye solution ML51 used for mode-locking. In the amplifier chain, the output semi-train of pulses from the pulse selector is amplified 20 times in the last (double) amplifier. The output energy of the laser system is 80 mJ in a spot size of about 5 mm diameter[19].

Characterization of the samples

After preparation of the three ZnO samples by the method described earlier in the text, they were characterized

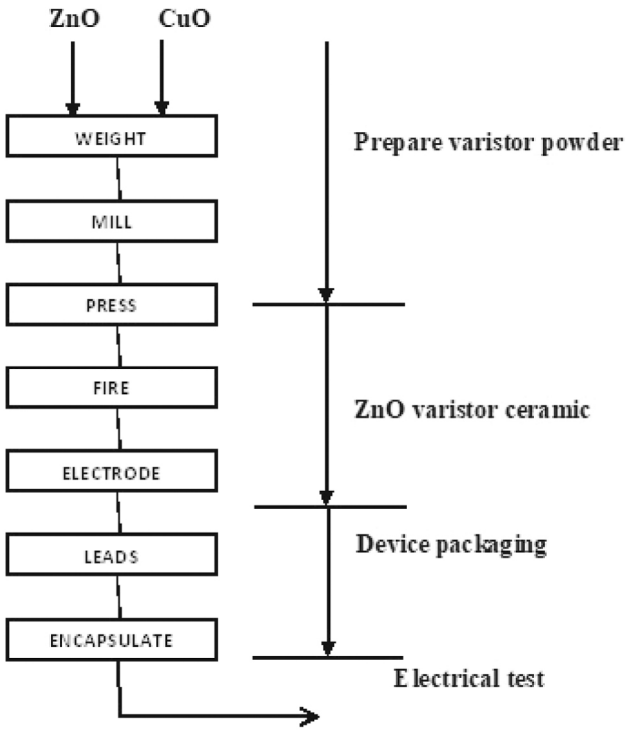

Figure 1. Block diagram showing different stages of preparation of ZnO varistors doped with copper oxide.

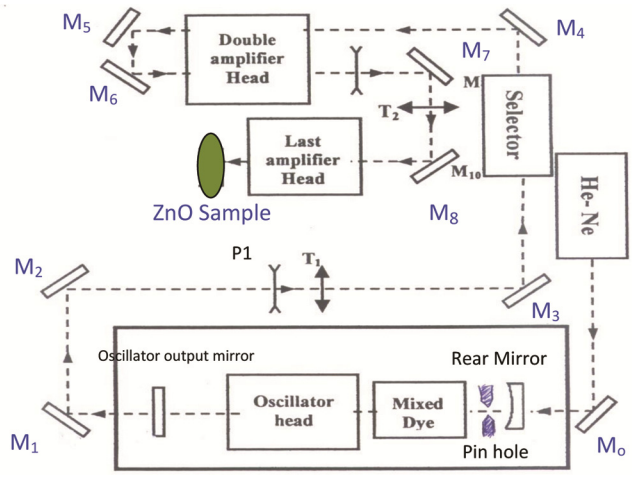

Figure 2. Block diagram showing the complete Nd : YAG laser system used for irradiating the three ZnO samples.

using three powerful tools – XRD, SEM and AFM, both before and after laser irradiation. XRD was carried out in transmission mode, where the sample was kept between two Kapton foils. This holder is especially advantageous when a sample cannot be ground fine for use in capillaries. Transmission measurements are a valuable tool for obtaining good quality diffraction data for unit cell determination, despite the intrinsically lower-peak-to background ratio compared to standard Bragg–Brentano geometry. A diffractometer (PANalytical X'Pert PRO) was used whose goniometer: PW3050/60 of 240.00 mm radius, with minimum step size (2θ, degree) of 0.001; having minimum step size (Omega) of 0.001, X-ray wavelength of 1.54 Å, copper anode source and Ni-filter. Scan had a step time of 0.50 s and step size of 0.02 (2θ, degree), the divergence slit size was fixed at 0.4785°. The measurement temperature was 25.00°C; specimen length was 10.00 mm, receiving slit size was 0.10 mm and generator settings were 30 mA and 40 kV.

SEM surface characterization of the three samples was carried out using a SEM (Czech) and EDX apparatus (Quanta FEG250).

AFM data from the three samples were collected using a contact mode AFM (AutoProbe Cp-Research head, Thermo Microscope). The probe is a nonconductive silicon nitride (Bruker, model: MLCT-MT-A). Pro-scan 1.8 software was used for controlling the scan parameters and IP 2.1 software for image analysis; the scan area was $10 \times 10\ \mu m^2$ and the number of data points was 256×256 with scan rate of 1 Hz. The XPS spectrum was produced by the XPS (PHI 5000 Versa Probe II) having monochromatic X-ray source of Al-K_α ($h\nu = 1486.6$ eV) with spot size of 200 μm. An analyser of 187.85 eV having a power of 50 W was used. Multipack software (Version 9, ULVAC-PHI, Inc., Japan) was used to analyse the XPS data and for fitting of the Gaussian–Lorentzian line shapes, effects of spin–orbit splitting, surface composition, interface and depth analysis of ZnO.

Results and discussion

X-ray diffraction results

The peak list table shows the *hkl* values, planar distance *d* (Å) and relative peak intensity *I* (%) for 27 different values of 2θ angle ranging from 31.802° to 143.275° (Table 1).

The XRD pattern is of typically hexagonal ZnO with card number JCPDS: 36-1451 (ref. 20). It shows the following crystallographic parameters: space group: P63mc; space group number: 186; lattice parameters: *a* (Å): 3.2465, *b* (Å): 3.2465, *c* (Å): 5.2030, alpha: 90.0000°, beta: 90.0000°, gamma: 120.0000°, volume of cell: 47.49 $Å^3$.

Tables 2–4 show the measured parameters; 2θ, *d*, *I* and peak broadening full width at half maximum (FWHM) for samples (1–3) respectively, before laser irradiation.

The principal peaks are assigned 100% relative intensity, but changes in peak intensities for each sample in Tables 2–4 refer to many factors such as: incident beam intensity, distance from the specimen to the detector, wavelength of the X-radiation, linear attenuation coefficient of the specimen and volume fraction of phase α in the specimen.

For quantitative analysis, the preferred orientation is probably the most common cause of deviation of experimental diffractometer data from the 'ideal' intensity pattern for the phase(s) analysed. Preferred orientation can be recognized and compensated for when identifying crystalline phases in a specimen, but is much more difficult

Table 1. ZnO peak list table showing *hkl* values, planar distance *d* and relative peak intensities *I*

h	*k*	*l*	*d* (Å)	2θ (degree)	*I* (%)
1	0	0	2.81155	31.802	55.6
0	0	2	2.60150	34.447	41.0
1	0	1	2.47352	36.289	100.0
1	0	2	1.90948	47.583	21.4
1	1	0	1.62325	56.659	31.2
1	0	3	1.47609	62.913	27.7
2	0	0	1.40578	66.453	4.2
1	1	2	1.37715	68.021	22.7
2	0	1	1.35711	69.167	11.2
0	0	4	1.30075	72.626	1.8
2	0	2	1.23676	77.047	3.5
1	0	4	1.18053	81.461	1.8
2	0	3	1.09208	89.716	7.3
2	1	0	1.06267	92.916	2.4
2	1	1	1.04117	95.436	7.4
1	1	4	1.01506	98.730	4.0
2	1	2	0.98376	103.075	2.8
1	0	5	0.97590	104.244	5.1
2	0	4	0.95474	107.572	0.8
3	0	0	0.93718	110.557	3.2
2	1	3	0.90610	116.450	8.0
3	0	2	0.88171	121.768	4.3
0	0	6	0.86717	125.320	0.6
2	0	5	0.83639	134.142	3.7
1	0	6	0.82865	136.741	0.9
2	1	4	0.82295	138.788	1.2
2	2	0	0.81163	143.275	2.5

Table 2. 2θ, *d*-spacing, *I* and peak broadening full width at half maximum (FWHM) for sample 1

2θ (degree)	*d* (Å)	*I* (%)	FWHM
31.7401	2.81923	60.74	0.2952
34.4548	2.60307	24.54	0.2755
36.2603	2.47749	100	0.3149
47.5147	1.91364	16.28	0.3346
56.5488	1.6275	26.81	0.2952
62.8627	1.47837	16.47	0.2952
66.2928	1.40996	2.89	0.1574
67.912	1.38023	15.03	0.2558
69.0132	1.36088	7.46	0.2362
69.2786	1.35519	4.88	0.192

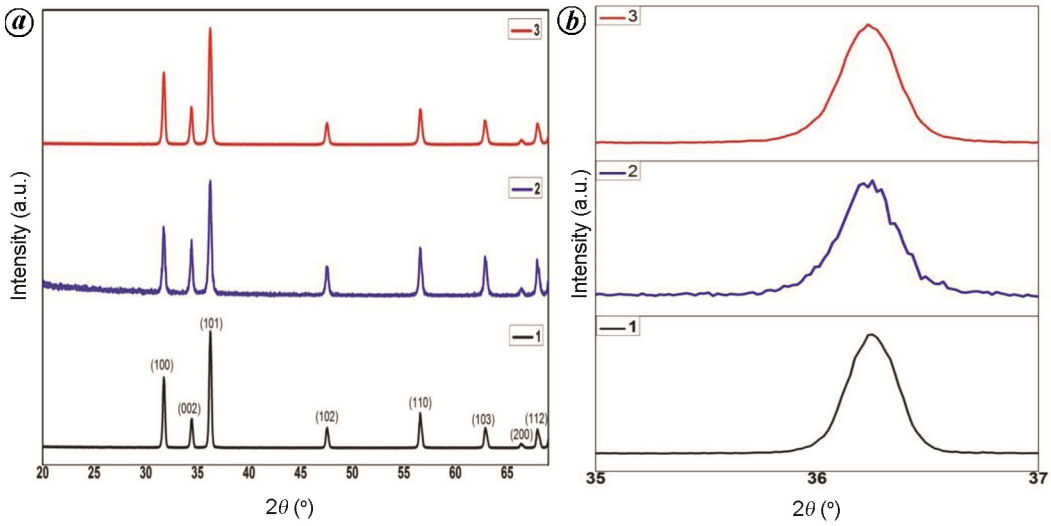

Figure 3. X-ray diffraction plots of ZnO varistor samples 1–3 doped with copper oxide before exposing them to laser radiation (***a***) and their expanded principal peaks (***b***).

Table 3. 2θ, *d*-spacing, *I* and peak broadening FWHM for sample 2

2θ (degree)	*d* (Å)	*I* (%)	FWHM
31.7434	2.81895	57.59	0.2755
34.4294	2.60493	40.89	0.2362
36.2266	2.47972	100	0.2952
47.5621	1.91184	25.26	0.2165
56.5529	1.62739	38.56	0.2362
62.8057	1.47958	27.8	0.2362
66.3373	1.40912	5.29	0.3149
67.899	1.38047	27.36	0.1968
69.0109	1.35979	14.67	0.264

to deal during quantitative analysis or precise unit cell calculations. The most common way of dealing with preferred orientation in a material of known composition is to compare the diffraction intensities of the specimen showing preferred orientation with the calculated (random) pattern for the material. Some data analysis software (including MDIs Jade with the appropriate add-on modules) will adjust data to correct for preferred orientation in a specimen[21].

The XRD plots in Figure 3 show Bragg peaks before laser irradiation from different crystalline planes at different 2θ values by varying the angle of the detector for the three samples (1–3) from bottom to up. The intensity of the reflected beam has sharp peaks; the scattered beams emerge only when the condition is met by a family of crystal planes, which is the Bragg condition for diffraction[22,23]. Figure 4 shows X-ray diffraction plots of the three samples after laser radiation (Figure 4 *a*) and their expanded principal peak (Figure 4 *b*).

It can be observed from Figure 3 that before laser irradiation, the average ZnO grain size does not depend too much on the CuO dopant amount because when the principal peak is expanded horizontally, no appreciable shifts are noticed between the principal peaks of the three samples. After laser irradiation, different shifts are noticed in the 2θ values of the three principal peaks of the samples (Figure 4). For sample (1), the principal peak shifts after laser irradiation from its original value before laser irradiation towards the higher 2θ direction, i.e. a decrease in the average grain size occurs. However for sample 2, a slight decrease towards the low 2θ direction is observed. This indicates higher average ZnO grain size in sample 2 after laser irradiation than before irradiation. For sample 3, a small shift is noticed in its principal peak but in the direction of higher 2θ, i.e. a decrease in the average ZnO grain size occurs in sample 3 after laser irradiation. The FWHM of each peak (β) measured in radians is a measure of the average vertical crystallite size (D) in a polycrystalline material as described and calculated from the Scherer's equation (eq. (1)), and listed in Tables 5–10 with their calculated dislocation coefficients.

$$D = 0.97\lambda/\beta\cos\theta, \tag{1}$$

where D is the average crystallite size in the vertical direction of the crystal, λ the X-ray wavelength (1.540 Å), θ is the Bragg angle (degree).

The dislocation coefficient (δ) is then calculated for each sample using the relation

$$\delta = 1/D^2. \tag{2}$$

Tables 5, 7 and 9 show the line broadening FWHM, the calculated average crystallite size (D), the inter-planar distances (d) and the calculated dislocation coefficient

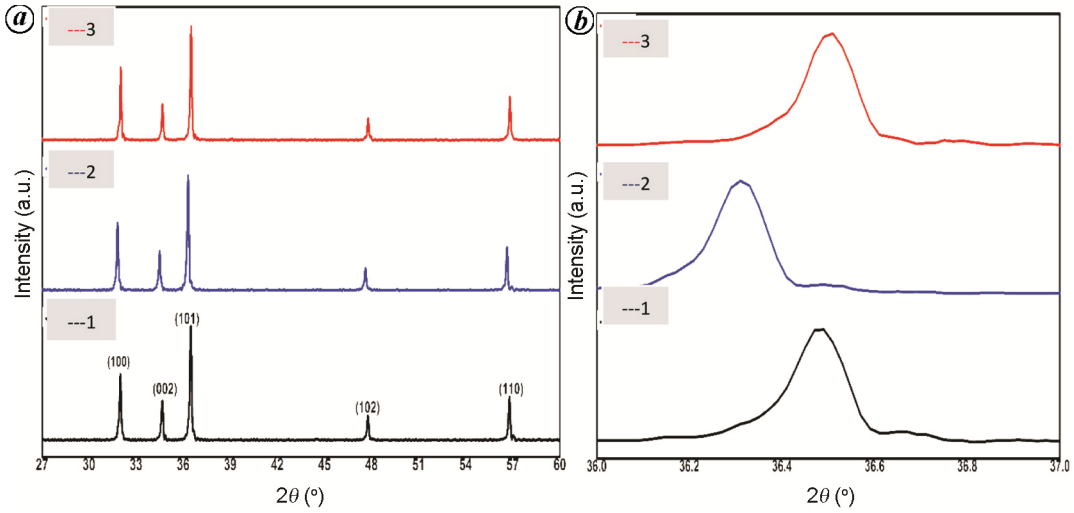

Figure 4. X-ray diffraction plots of ZnO varistor samples 1–3 doped with copper oxide after exposing them to laser radiation (***a***) and their expanded principal peaks (***b***).

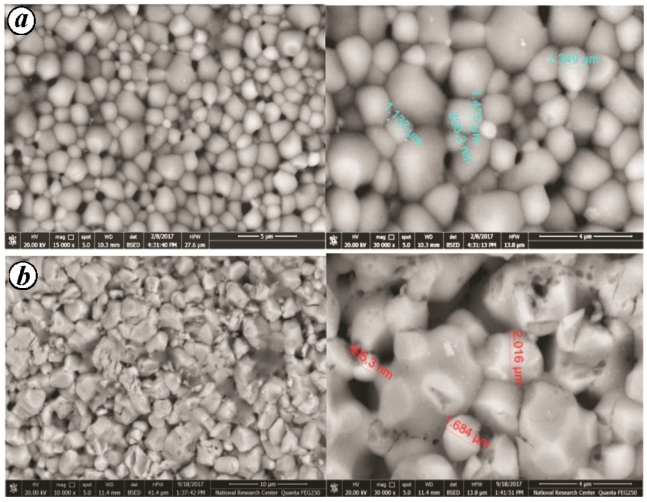

Figure 5. SEM images of ZnO sample 1. Before (***a***) and after (***b***) laser irradiation.

Table 4. 2θ, *d*-spacing, *I* and peak broadening FWHM for sample 3

2θ (degree)	*d* (Å)	*I* (%)	FWHM
31.7488	2.81848	61.48	0.3149
34.4317	2.60476	30.85	0.2558
36.2419	2.4787	100	0.3346
47.5044	1.91403	17.52	0.3542
56.5678	1.627	29.62	0.2952
62.8424	1.4788	19.86	0.2362
66.3169	1.4095	3.13	0.2362
67.9383	1.37862	17.38	0.288
68.2066	1.37726	8.4	0.216
69.0299	1.35946	8.64	0.336

(δ) before laser irradiation, while Tables 6, 8 and 10 show these values after laser irradiation for the first five peaks of samples (1–3) respectively.

The XRD patterns of the three ZnO samples doped with CuO show well-defined peaks located at Bragg angles. The five most intensive characteristic peaks studied corresponding to the planes with Miller indices of (100), (002), (101), (102) and (110) respectively, indicate that the samples have a good crystalline nature. XRD patterns confirm the ZnO hexagonal structure. Comparison between the calculated crystallite size *D* (Tables 5–10) before and after laser irradiation shows a large increase in the average crystallite size – more than twice the original values before laser irradiation in all samples. For example, the crystallite size of sample 1 was 30.1 nm before irradiation and increased to become 74.26 nm after laser irradiation. Therefore, a large decrease in average dislocation coefficients occurs by laser irradiation, as they are inversely proportional to D^2.

SEM results

The resulting SEM images in Figures 5–7 for samples 1–3 respectively, show their surface morphology.

The presence of inter-granular phase, and additives present in the grain boundaries between ZnO grains are clear in sample 3, as CuO content has the largest value (3.0 mol%) than the two other samples. Also, comparing images for samples 1 and 2, Figures 5 *a* and 6 *a* before laser irradiation reveal that increasing CuO from 0.5 to 1.0 mol% causes a significant increase in grain size in sample 2, which indicates a decrease in the distortion parameter. High periodicity and grain hexagonal structure are clear from SEM images for the three samples before laser irradiation. Some pores also appear in the grains and the inter-granular distances significantly increase as a result of laser irradiation. In sample 2, however, grain melting and particulate formation with the increase of

Table 5. *hkl* values, 2θ, *d*-spacing, FWHM, calculated crystallite size (*D*) and dislocation δ before laser irradiation for sample 1

hkl	2θ (degree)	*d* (Å)	FWHM (degree)	*D* (nm)	$\delta \times 10^{-3}$ (nm)$^{-2}$
1 0 0	31.7401	2.81923	0.2952	30.16	1.1
0 0 2	34.4548	2.60307	0.2755	32.56	0.94
1 0 1	36.2603	2.47749	0.3149	28.62	1.22
1 0 2	47.5147	1.91364	0.3346	27.95	1.28
1 1 0	56.5488	1.62750	0.2952	32.93	0.92

Table 6. *hkl* values, 2θ, *d*-spacing, FWHM, *D* and δ after laser irradiation for sample 1

hkl	2θ (degree)	*d* (Å)	FWHM (degree)	*D* (nm)	$\delta \times 10^{-3}$ (nm)$^{-2}$
1 0 0	31.999	2.794	0.12	74.26	0.181
0 0 2	34.683	2.584	0.144	62.32	0.257
1 0 1	36.494	2.460	0.144	62.64	0.255
1 0 2	47.775	1.902	0.144	65.05	0.236
1 1 0	57.062	1.612	0.096	101.55	0.097

Table 7. *hkl* values, 2θ, *d*-spacing, FWHM, *D* and δ before laser irradiation for sample 2

hkl	2θ (degree)	*d* (Å)	FWHM (degree)	*D* (nm)	$\delta \times 10^{-3}$ (nm)$^{-2}$
1 0 0	31.7434	2.81895	0.2755	32.31	0.96
0 0 2	34.4294	2.60493	0.2362	37.95	0.69
1 0 1	36.2266	2.47972	0.2952	30.52	1.07
1 0 2	47.5621	1.91184	0.2165	43.22	0.54
1 1 0	56.5529	1.62739	0.2362	40.88	0.60

Table 8. *hkl* values, 2θ, *d*-spacing, FWHM, *D* and δ after laser irradiation for sample 2

hkl	2θ (degree)	*d* (Å)	FWHM (degree)	*D* (nm)	$\delta \times 10^{-3}$ (nm)$^{-2}$
1 0 0	31.824	2.810	0.120	74.23	0.181
0 0 2	34.500	2.597	0.120	74.73	0.179
1 0 1	36.319	2.471	0.144	62.61	0.255
1 0 2	47.612	1.908	0.120	87.01	0.132
1 1 0	56.635	1.623	0.144	67.57	0.219

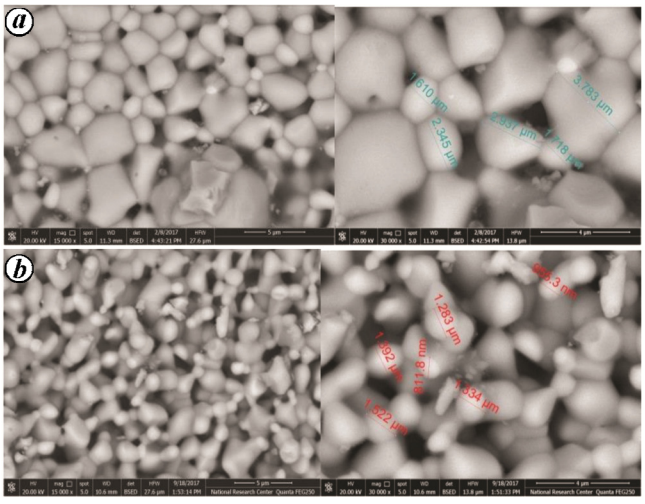

Figure 6. SEM images of ZnO sample 2; before (***a***) and after (***b***) laser irradiation.

inter-granular distances compared to the newly formed particulate sizes are more obvious than in sample 1 without the appearance of pores in the new particulates, which indicates total melting of the grains. These results lead to the fact that ZnO grains in all samples have been decomposed because the formation of particulates is target material-dependent, and when the target material contains oxygen gas, the irradiated surfaces might become oxygen-free by laser heating.

AFM results

AFM data generate quantitative information from individual particles and between groups of particles, which can allow precise analyses of maximum diameter, mean radius, perimeter, surface area, volume, distortion and roughness of particles. Figures 8–10 show the three- and

Table 9. *hkl* values, 2θ, *d*-spacing, FWHM, *D* and δ before laser irradiation for sample 3

hkl	2θ (degree)	*d* (Å)	FWHM (degree)	*D* (nm)	$\delta \times 10^{-3}$ (nm)$^{-2}$
1 0 0	31.7488	2.81848	0.3149	28.27	1.25
0 0 2	34.4317	2.60476	0.2558	35.04	0.81
1 0 1	36.2419	2.4787	0.3346	26.92	1.38
1 0 2	47.5044	1.91403	0.3542	26.41	1.46
1 1 0	56.5678	1.627	0.2952	32.94	0.92

Table 10. *hkl* values, 2θ, *d*-spacing, FWHM, *D* and δ after laser irradiation for sample 3

hkl	2θ (degree)	*d* (Å)	FWHM (degree)	*D* (nm)	$\delta \times 10^{-3}$ (nm)$^{-2}$
1 0 0	32.028	2.792	0.120	74.27	0.181
0 0 2	34.685	2.584	0.120	74.78	0.179
1 0 1	36.509	2.459	0.144	59.75	1.380
1 0 2	47.790	1.901	0.120	78.07	0.164
1 1 0	56.818	1.61908	0.120	81.15	0.152

Table 11. Average values of mean radius, maximum diameter, perimeter, distortion coefficient and roughness for the three samples before laser irradiation

Sample	Mean radius (μm)	Maximum diameter (μm)	Perimeter (μm)	Distortion coefficient	Roughness (nm)
1	0.080	0.249	0.622	0.739	1.586
2	0.092	0.306	0.737	0.548	1.885
3	0.083	0.233	0.623	0.769	1.326

Table 12. Atomic force microscope (AFM) data from the three samples before laser irradiation

	Sample		
Parameters	1	2	3
Rp-v (μm)	0.834	0.186	0.960
RMS rough (Rq) (μm)	0.114	0.107	0.113
Ave rough (Ra) (μm)	0.093	0.083	0.086
Mean height (μm)	0.538	1.500	0.461
Median height (μm)	0.533	1.506	0.462
Bearing ratio at 20.0% (μm)	0.643	1.59	0.555
Bearing ratio at 80.0% (μm)	0.433	1.41	0.377
Peak (μm)	0.296	1.41	0.498
Valley (μm)	–0.537	–1.500	0.461
Volume (μm^3)	53.77	150.0	46.15
Surface area (μm^2)	108.0	110.2	104.8
Projected area (μm^2)	100.0	100.0	100.0

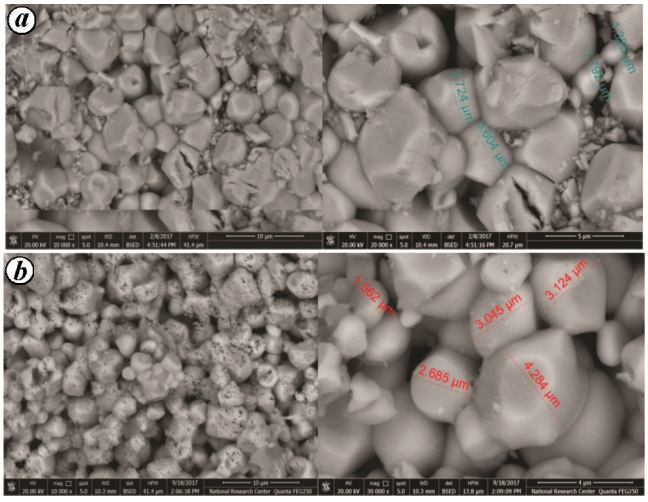

Figure 7. SEM images of ZnO sample 3; before (***a***) and after (***b***) laser irradiation.

two-dimensional AFM images for ZnO samples 1–3 respectively, before and after laser irradiation.

Comparison between AFM images for the three samples before laser irradiation reveals the change in some surface morphology parameters, such as grain size for the three samples according to the percentage of CuO. Therefore, different surface morphology parameters appear as well between the three samples after laser irradiation, which is clear from the values of mean radius, maximum diameter, perimeter, distortion coefficient and roughness for the samples (Table 11). Tables 12 and 13 show AFM data from these samples before and after laser irradiation respectively.

Table 11 shows that roughness is maximum for sample 2, which has CuO content of 1 mol%, and is lowest for sample 3 with 3 mol% content of CuO, while sample 1 (which has the lowest content of CuO, 0.5 mol%) has an intermediate roughness value as well as intermediate

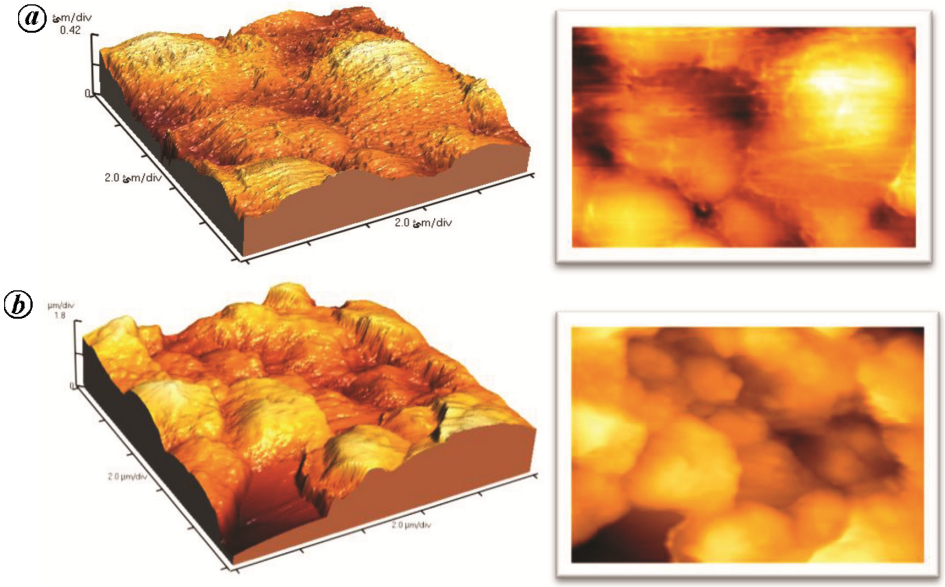

Figure 8. Three- and two-dimensional AFM images for ZnO sample 1, before (***a***) and after (***b***) laser irradiation.

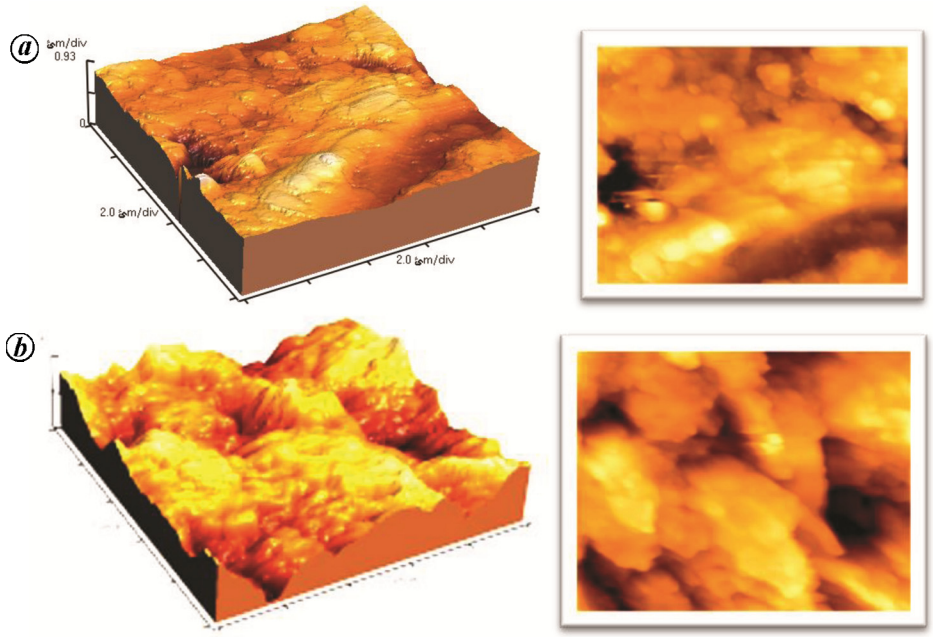

Figure 9. Three- and two-dimensional AFM images for ZnO sample 2, before (***a***) and after (***b***) laser irradiation.

distortion coefficient, perimeter and maximum diameter compared with the other two samples of higher CuO content.

The roughness of the three samples increases after laser irradiation as seen in the tables; for example, it is 0.093 µm for sample 1 before laser irradiation and became 0.455 µm after irradiation.

XPS results

As an example, the XPS of sample 1 before laser irradiation is shown in Figure 11 and Table 14 shows the quantification parameters such as the peak element, position, FWHM and atomic concentrations.

Figure 11 shows elemental composition of the upper layer of ZnO varistor. In addition to Zn and oxygen and Cu dopant peaks, we also observe some carbon peaks on the upper surface of the multilayer. Zn 2p3/2 peak is found at 1020.750 eV (Table 14), which indicates formation of the Zn–O bond. Survey spectra in Figure 11 show sharp peaks of C 1s at 284.00 eV, which could be attributed to the graphitic carbon impurity in the sample, O 1s at 529.750 eV, Zn 2p3/2 observed at 1020.750 eV and Cu 2p at 933.250 eV which provides evidence of Cu(I). While Cu(I) was found to be 98.55%, Cu(II) was 1.45%

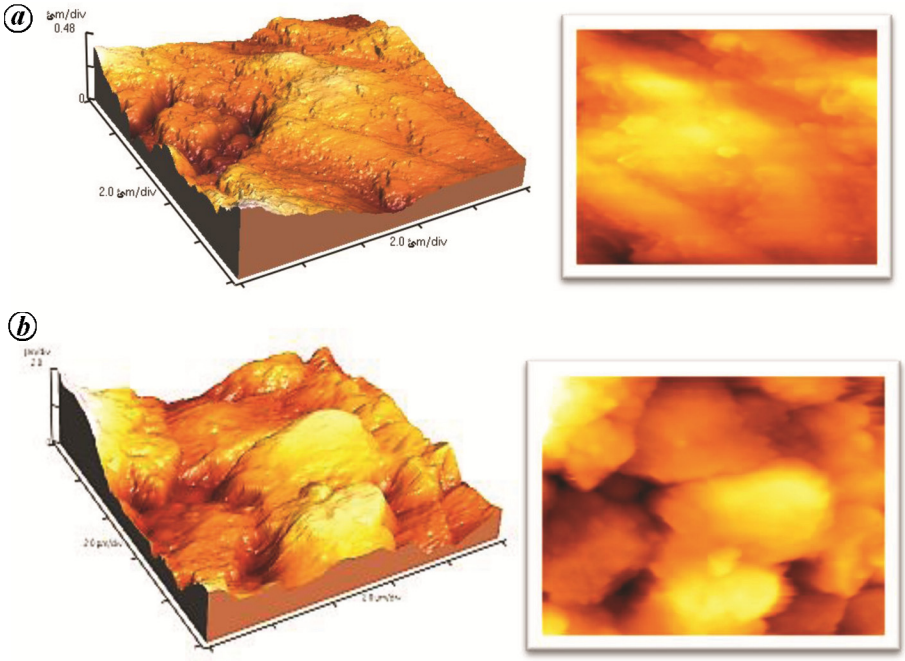

Figure 10. Three- and two-dimensional AFM images for ZnO sample 3, before (***a***) and after (***b***) laser irradiation.

Table 13. AFM data from the three samples after laser irradiation

Parameters	Sample		
	1	2	3
Rp-v (μm)	3.566	2.368	4.047
RMS rough (Rq) (μm)	0.575	0.389	0.608
Ave rough (Ra) (μm)	0.455	0.309	0.486
Mean height (μm)	2.249	1.267	1.472
Median height (μm)	2.290	1.309	1.416
Bearing ratio at 20.0% (μm)	2.76	1.60	1.97
Bearing ratio at 80.0% (μm)	1.80	0.947	0.946
Peak (μm)	1.317	1.101	2.575
Valley (μm)	–2.249	1.267	–1.472
Volume (μm^3)	224.9	126.7	147.2
Surface area (μm^2)	168.9	158.5	171.3
Projected area (μm^2)	100.0	100.0	100.0

in the chemical state of Cu 2p3/2. The shake-up line in Cu 2p3/2 spectra indicates the presence of Cu(II). The presence of Zn 2p3/2, Zn 2p1/2 and O 1s peaks at 1020.750, 1035.2 and 529.750 eV respectively, confirm again that the samples are ZnO. Figure 11 also shows sharp peaks of Ca 2p at 346.250 eV and Cr 2p at 575.500 eV; Si 2s peak was detected at 152.000 eV. Other values, such as FWHM are useful indicators of chemical-state changes and physical influences; that is, broadening of a peak may indicate a change in the number of chemical bonds contributing to a peak shape, and change in the sample condition. Sensitivity factors are used to scale the measured peak areas, so variations in the peak areas are representative of the amount of material on the surface (through depth of about 10 μm) of the sample. The spectrum is dominated by two photoelectron peaks, corresponding to electrons originating in the 1s orbitals of the carbon and oxygen atoms in the sample surface. The atomic concentration ratio of elements measured by XPS is expected to be different from that measured by EDX because for the latter, penetration depth is much greater than for the former.

Conclusion

XRD shows the ZnO hexagonal structure before and after laser irradiation the average crystallite size increased. Inter-granular phase and presence of CuO molecules between ZnO grains are observed in the SEM images before laser irradiation. SEM images show a noticeable decrease in grain size after laser irradiation, and production of pores, cracks and particulates of dimensions in the submicron range. The number of cracks increases after laser irradiation for 2 min. The laser-induced grain melting, pores, cracks and particulates increase the surface roughness for the three samples. The large increase in the roughness is observed due to laser irradiation depending on the nature of the plasma formed above the material by the high intensity laser. This plasma imparts energy to the surface of the irradiated area leading to surface melting of the area, as can be seen in the SEM images.

The XPS through a depth of about 10 μm from the surface for sample 1 reveals Zn 2p3/2 peak at 1020.750 eV, C 1s at 284.00 eV, O 1s at 529.750 eV and Cu 2p at

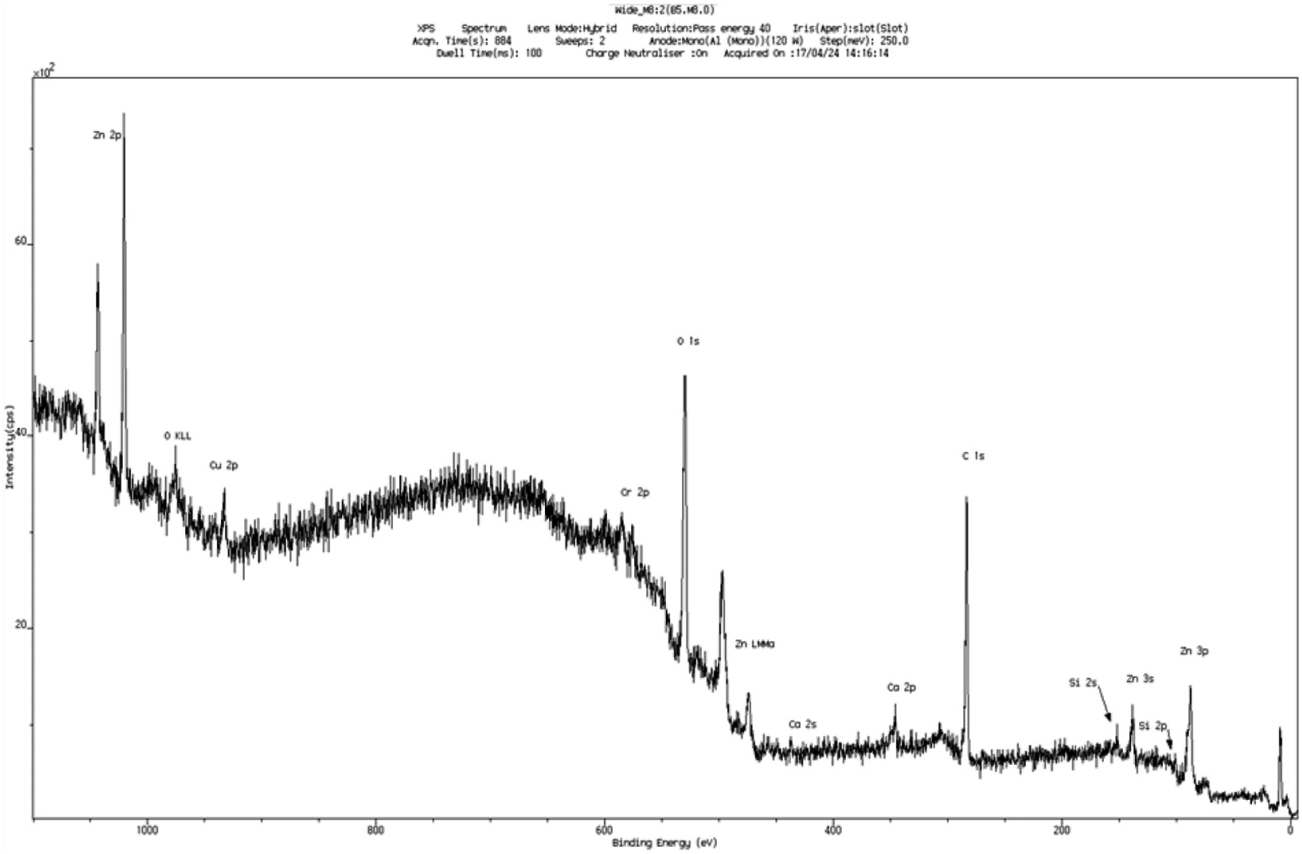

Figure 11. X-ray photoelectron spectra of ZnO varistor doped with CuO.

Table 14. Quantification parameters

Peak	Type BE (eV)	Position (eV)	FWHM (cps eV)	Raw area	RSF mass	Atomic (conc%)	Atomic (conc%)	Mass
Zn 2p	Reg	1020.750	1.755	11850.9	5.589	65.387	5.35	17.58
Cu 2p	Reg	933.250	1.743	6966.9	5.321	63.549	3.46	11.04
Cr 2p	Reg	575.500	0.544	2495.0	2.427	51.996	2.78	7.27
O 1s	Reg	529.750	2.969	9248.8	0.780	15.999	32.14	25.84
Ca 2p	Reg	346.250	1.512	1633.8	1.833	40.078	2.40	4.83
C 1s	Reg	284.000	1.843	5402.5	0.278	12.011	52.72	31.82
Si 2s	Reg	152.000	0.559	141.2	0.324	28.086	1.15	1.62

PS, For try position +1.5 eV.

933.250 eV, indicating the presence of Cu(I). The shake-up line in Cu 2p3/2 spectra indicates the presence of Cu(II); Cu(I) is found 98.55% while Cu(II) is 1.45% in the chemical state of Cu 2p3/2. Sharp peaks of Ca 2p are seen at 346.250 eV and Cr 2p at 575.500 eV; Si 2s peak is detected at 152.000 eV.

Future work will focus on how these effects of laser irradiation could change the nonlinear electrical properties of ZnO varistors, as their electrical properties are highly dependent on their microstructure and surface morphology[24].

1. Overschelde, O. V. *et al.*, *J. Appl. Phys.*, 2008, **104**, 103106.
2. Overschelde, O. V., Guisbiers, G. and Wantelet, M., *J. Phys. Chem. C*, 2009, **113**, 15343–15345.
3. Lu, H. *et al.*, Effects of laser irradiation on the structure and optical properties of ZnO thin films. *Mater. Lett.*, 2010, **64**, 2072–2075.
4. Pauleau, I., *Material Surface Processing by Directed Energy Techniques*, Elsevier, 2005.
5. Pradhan, B., Batabyal, S. K. and Pal, A. J., *Sol. Energy Mater. Sol. Cells*, 2007, **91**, 769–773.
6. Wang, M. R., Wang, J., Chen, W., Cui, Y. and Wang, L. D., *Mater. Chem. Phys.*, 2006, **97**, 219–225.
7. Nahm, C. W., *Mater. Lett.*, 2008, **62**, 4440–4442.
8. Wan, Q., Li, Q. H., Chen, Y. J., Wang, T. H. and He, X. L., *Appl. Phys. Lett.*, 2004, **84**, 3654–3656.
9. Alexander, W. and Street, A., *Metals in the Service of Man*, 1985, 8th edn.

10. Hoppe, M. *et al.*, (CuO–Cu_2O)/ZnO : Al heterojunctions for volatile organic compound detection. *Sensor. Actuat. B*, 2018, **255**(2), 1362–1375.
11. Razali, N. Z., Abdullah, A. H. and Haron, M. J., Synthesis of CuO and ZnO nanoparticles and CuO doped ZnO nanophotocatalysts. *Adv. Mater. Res.*, 2012, **364**, 402–407.
12. Mansour, S. E., Desouky, O. A., Najar, A. M. and Negim El-Sayed, M., Sakhy, M. and Mun, G. A., Effect of temperature on the characteristics of zinc oxide with cerium oxide at constant frequency (20 kHz). *Euro. J. Appl. Sci.*, 2013, **5**(3), 100–106.
13. Jianga, F., Penga, Z., Zanga, Y. and Fub, X., Progress on rare-earth doped ZnO-based varistor materials. *J. Adv. Ceram.*, 2013, **2**(3), 201–212.
14. Matsuoka, M., *Jpn. J. Appl. Phys.*, 1971, **10**, 736.
15. Saadeldin, M. M. *et al*., Study of the electrical properties and the microstructure of ZnO varistors doped with CuO and Na_3BiO_3m, 2015.
16. Steele, P. C. H., *Applied Science*, Elsevier, A. Iagrange, 1993, p. 1.
17. Ibrahim, M., Hanna, Y. S., Samwel, S. W. and Hegazy, M. A., Satellite laser ranging in Egypt. *NRIAG J. Astron. Geophys.*, 2015, **4**(1), 123–129.
18. Ibrahim, M., 17 years of ranging from the Helwan-SLR station. *Astrophys. Space Sci. J.*, 2011, **335**, 379–387.
19. Mansour, H. M., Khalil, A. A. I., Helali, M. Y. and Mansour, M., Development of the stability on the laser system used at satellite laser ranging station. *J. Nucl. Part. Phys.*, 2014, **4**(1), 7–16.
20. Yoshio, K., Onodera, A., Satoh, H., Sakagami, N. and Yamashita, H., *Ferroelectrics*, 2001, **264**, 133.
21. Connolly, J. R., Diffraction Basics, Part 2, for EPS400-002, Introduction to X-Ray Powder Diffraction, 2012.
22. Warren, B. E., *X-Ray Diffraction*, Addison-Wesley, 1969.
23. Grieken, R. and Markowicz, A., *Handbook of X-Ray Spectrometry*, CRC Press, Boca Raton, FL, 2002, 2nd edn.
24. Saadeldin, M. M., Younis, M. M., Ahmed, M. M. and Helali, M. Y., The effect of firing temperature on the electrical properties and the microstructure of ZnO varistors doped with CuO. *Indian J. Appl. Res.*, 2015, **5**(10).

Received 13 January 2019; revised accepted 5 February 2019

doi: 10.18520/cs/v116/i11/1818-1828